Journal of Applied Electrochemistry **29**: 1423–1426, 1999.

Electrochemical study on orthorhombic $LiMnO_2$ as cathode in rechargeable lithium batteries

G.X. WANG*, P. YAO, S. ZHONG, D.H. BRADHURST, S.X. DOU and H.K. LIU
Energy Storage Materials Program, Institute for Superconducting & Electronic Materials, University of Wollongong, NSW 2522, Australia
*(*author for correspondence, e-mail: gw14@uow.edu.au)*

Received 2 February 1999; accepted in revised form 19 May 1999

Key words: a.c. impedance spectroscopy, orthorhombic $LiMnO_2$, rechargeable lithium battery

Abstract

Orthorhombic $LiMnO_2$ was synthesized via a solid-state reaction. Its electrochemical properties as cathode in lithium batteries were examined. It was found that initially, a few cycles are necessary to activate the electrochemical reactivity of *o*-$LiMnO_2$, which is related to the transformation from the orthorhombic phase to a spinel-like phase. A maximum discharge capacity of 180–190 mA h g^{-1} for *o*-$LiMnO_2$ electrodes was achieved. An electrochemical impedance spectroscopy (EIS) study showed that the charge-transfer resistance (R_{CT}) for the initial *o*-$LiMnO_2$ electrode is much larger than that for the *o*-$LiMnO_2$ electrode in the charged state. The *o*-$LiMnO_2$ electrode demonstrated a better cyclability than that of the spinel $LiMn_2O_4$ directly synthesized by solid-state reaction.

1. Introduction

The Li–Mn–O system is the most intensively investigated cathodic materials for rechargeable lithium batteries. The spinel $LiMn_2O_4$ has several advantages over $LiCoO_2$ and $LiNiO_2$ such as high voltage, low cost and low toxicity. However, it suffers from low capacity (a theoretical capacity of only 148 mA h g^{-1} compared to 274 mA h g^{-1} for layered $LiCoO_2$) and short cycle life [1–4]. The search for layered $LiMnO_2$ with the same structure as $LiCoO_2$ is currently being pursued. Recently, the synthesis and electrochemical properties of layered $LiMnO_2$ (monoclinic c2/m, or *m*-$LiMnO_2$) by an ion-exchange method has been reported [5]. The *m*-$LiMnO_2$ was found to be intolerant to lithium ion extraction/insertion, although its first charge capacity can reach 270 mA h g^{-1}. Another class of $LiMnO_2$ compounds (orthorhombic, Pmnm) or *o*-$LiMnO_2$ can be synthesized by solid-state reaction both at high and low temperature. A capacity in the range of 50 mA h g^{-1} to 200 mA h g^{-1} has been demonstrated with good cyclability [6–11]. *o*-$LiMnO_2$ was observed to transform to spinel-like $LiMn_2O_4$ when cycled in the voltage window of 2.2–4.4 V in the first cycle. This has been confirmed by *ex situ* and *in situ* X-ray diffraction [12, 13]. The rechargeability of the electrochemically formed spinel-like materials in the voltage window of 2.2–4.4 V is much better than that of directly synthesized spinel $LiMn_2O_4$. Nevertheless, the kinetic process of Li ion insertion/extraction in the *o*-$LiMnO_2$ electrode has not been reported so far.

In this investigation, the orthorhombic $LiMnO_2$ was synthesized and its electrochemical performance as cathode was examined. The morphology of *o*-$LiMnO_2$ before and after cycling were observed by TEM. The kinetic parameters of Li ion insertion and extraction in *o*-$LiMnO_2$ were determined by a.c. impedance spectroscopy.

2. Experimental details

The *o*-$LiMnO_2$ compounds were synthesized with the precursors of $LiOH.H_2O$ (99.95%, Aldrich) and Mn_2O_3 (99%, Aldrich). The mixtures were fired at 450 °C for 5 h, thoroughly ground after cooling and then heated at 600 °C for 12 h. The heat treatment was carried out in a tube furnace with argon flow. The sample was nominally nonstoichiometric, prepared with a molar ratio of Li:Mn = 1.1:1 in precursors, in which the stacking faults were intentionally induced to improve its electrochemical reactivity according to [12] and [14]. X-ray diffraction was performed on the synthesized samples using a Phillip PW1010 diffractometer with a CuK_α radiation.

CR2032 coin cells were fabricated to test the electrochemical performance of *o*-$LiMnO_2$ as cathode in the lithium cells using a hand operated closing tool (Hohsen Corp., Japan). The hardware of CR2032 coin cell was provided by Hohson Corp., Japan. The cathode was made by dispersing the mixture of 85 wt % active materials, 10 wt % carbon black and 5 wt % PVDF binder into dimethyl phthalate to obtain a slurry. The

slurry was spread on to aluminium foil (15 mm in diameter) and then dried at 150 °C for 24 h. The electrolyte was 1 M $LiPF_6$ (lithium hexafluorophosphate) in a mixture of EC (ethylene carbonate) and DMC (dimethyl carbonate). The cells were assembled in an argon filled glove-box (Unilab, Mbraun, USA) in which the oxygen and moisture were controlled less than 1 ppm. The kinetic process of the *o*-$LiMnO_2$ electrode in each lithium cell was characterized by a.c. impedance spectroscopy using an EG&G PAR electrochemical impedance analyser (model 6310). The a.c. amplitude was 5 mV. The frequency range was from 65 kHz to 0.01 Hz. The lithium test cells for the EIS experiments consisted of a three electrode system in which lithium metal was used as both counter electrode and reference electrode. The configuration of the three electrode cell is the same as described in [15]. During the EIS test, the test cells were enclosed in the glove-box while connected by a sealed electrical strip to the a.c. impedance analyser.

3. Results and discussion

The X-ray diffraction pattern of the *o*-$LiMnO_2$ compounds is shown in Figure 1. All peaks are indexed by assuming an orthorhombic phase with a space group Pmnm. The lattice constants were refined against an internal silicon standard using a least square method with 20 diffraction peaks. The parameters of the unit cell were calculated as $a = 457.46$ pm, $b = 575.06$ pm and $c = 280.59$ pm, which is in good agreement with JCPDS 35-749. The impurity phase $LiMn_2O_4$ was present in the synthesized sample. Broadened peaks were observed, which could be caused by stacking faults in the crystal structure.

Li/*o*-$LiMnO_2$ coin cells were fabricated. Voltages for the freshly assembled cells were in the range 3.15–3.25 V. The Li/*o*-$LiMnO_2$ cells were cycled within the range 2.2–4.3 V at a constant current density of 0.2 mA cm^{-2} ($C/15$ rate). The first charge curve of one of these cells is shown in Figure 2. The *o*-$LiMnO_2$ electrode was quickly charged from o.c.v. to 3.6 V and then followed an ascending slope between 4.0 and 4.3 V.

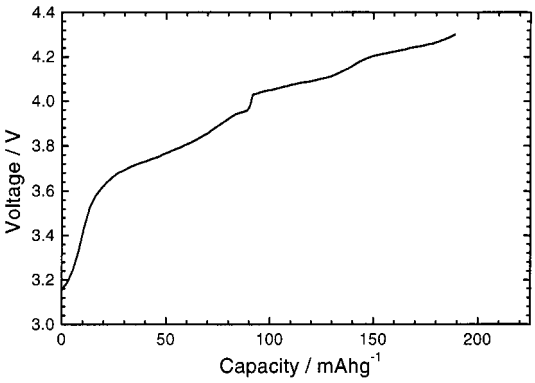

Fig. 2. First charge curve of the *o*-$LiMnO_2$ electrode.

An approximate 180 mA h g^{-1} capacity can be delivered by the *o*-$LiMnO_2$ electrode in the first charge, which is larger than that of the spinel $LiMn_2O_4$ electrode. It was found that a few cycles were necessary to activate the electrochemical reactivity of the *o*-$LiMnO_2$ electrode. Four to fifteen cycles were required at a $C/15$ rate before the maximum capacity was reached for different individual electrodes. The optimum discharge capacity for *o*-$LiMnO_2$ is in the range 180–190 mA h g^{-1}.

Figure 3 shows the discharge profile of a Li/*o*-$LiMnO_2$ cell at the fourth cycle, at which it delivered a maximum discharge capacity of 185 mA h g^{-1}. Two obvious discharge plateaus with constant voltage regions near to 4 V and 3 V, respectively, were observed, which is the characteristic of the spinel $LiMn_2O_4$ electrode [16]. The 4 V discharge plateau corresponds to Li intercalation into octahedral sites and the 3 V discharge plateau is associated with Li insertion into tetrahedral sites [12]. The 4 V discharge plateau is divided into two subplateaux, which is related to the reordering of Li in the structure when half of the Li ions were inserted.

The differential chronopotentiometric curve as shown in Figure 4 provides further evidence to support the above point. Reduction peaks are observed at 4.14, 4.02 and 2.91 V, respectively, which is exactly the same as for the spinel $LiMn_2O_4$ electrode. It appears that *o*-$LiMnO_2$ phases were gradually electrochemically transformed to

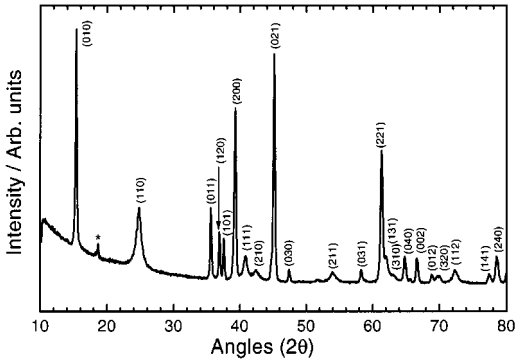

Fig. 1. X-ray pattern for the *o*-$LiMnO_2$ electrode. * impurity phase $LiMn_2O_4$.

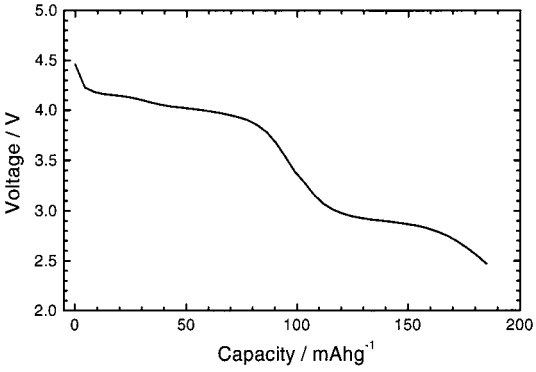

Fig. 3. Fourth discharge profile of a Li/*o*-$LiMnO_2$ cell, at which the maximum capacity was reached.

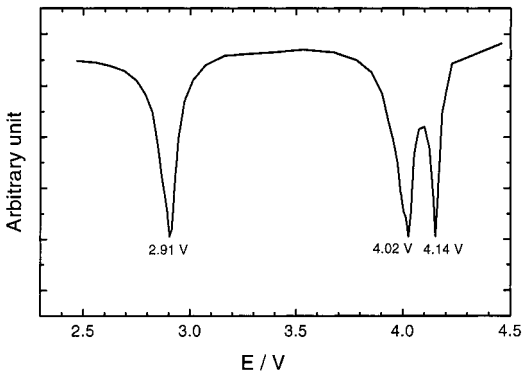

Fig. 4. Differential chronopotentiometric curve corresponding to Figure 3.

the spinel-like $LiMn_2O_4$ during charge/discharge cycle. From the analysis of XRD, we know that there are spinel $LiMn_2O_4$ impurity phases and stacking faults in the *o*-$LiMnO_2$ compounds. These spinel $LiMn_2O_4$ phases could be the nucleus for the nucleation of the spinel-like $LiMn_2O_4$ during cycling. This phenomenon has been confirmed via the *in situ* XRD analysis by Kötschau and Dahn [13]. It was considered that the *o*-$LiMnO_2$ was completely transformed to the spinel-like phase when it reached its maximum capacity.

Figure 5 shows the discharge capacity against the cycle number. The *o*-$LiMnO_2$ electrode demonstrated good cyclability, which is different from that of the spinel $LiMn_2O_4$. It is well known that the spinel $LiMn_2O_4$ electrode suffers from short cycle life due to the Jahn–Teller distortion [17]. This means that the electrochemically formed spinel-like phase originated from *o*-$LiMnO_2$ is more tolerant to cycling. The definitive mechanism is still unknown. However, TEM observation can provide some useful information. Figure 6 shows two TEM micrographs of *o*-$LiMnO_2$ before cycling (as prepared powders) and after 80 cycles. The morphology of crystal particles was not found to be significantly changed, which is beneficial in long term cycling of the electrode.

The Li/$LiMnO_2$ cells were also cycled at different current densities. Figure 7 compares the maximum

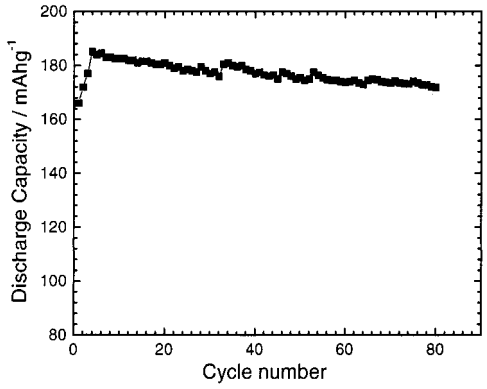

Fig. 5. Discharge capacity against cycle number of a Li/*o*-$LiMnO_2$ cell.

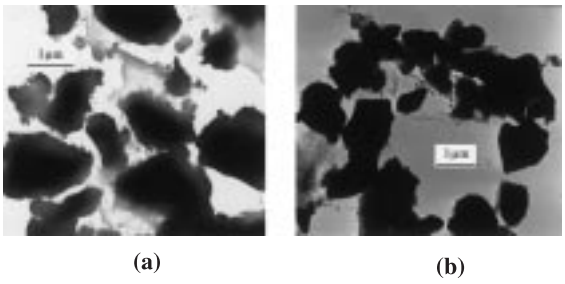

Fig. 6. TEM micrographs of *o*-$LiMnO_2$. (a) The as-prepared powders (before cycling) and (b) after 80 cycles.

discharge capacities at different discharge rates. The capacity of the *o*-$LiMnO_2$ electrode is sensitive to the charge/discharge rate, in agreement with the kinetic limitation. The slower the discharge rate, the higher the capacity. By contrast, the slower the cycle rate, the less cycle numbers are needed to reach the maximum capacity.

The electrochemical impedance spectroscopy (EIS) is a powerful tool to characterise the kinetics of the electrode process. The a.c. impedance spectra of *o*-$LiMnO_2$ electrode at different state-of-charge (SOC) were obtained and two typical Nyquist plots are present in Figure 8. A semicircle is centered on the real axis at high frequencies from which the charge transfer resistance R_{CT} can be deduced. Consequently, the exchange current density i_o can be calculated from the formula: $i_o = RT/nFR_{CT}$. In the low frequency range, a straight line at 45° to the real axis corresponds to the Warburg impedance [18]. The R_{CT} of *o*-$LiMnO_2$ at 0% SOC (3.25 V) state was 76.5 $\Omega\,cm^{-2}$ (corresponding an exchange current density $i_o = 3.3 \times 10^{-4}$ A cm^{-2}). This is much larger than that in the 90% SOC charged state (4.2 V) $R_{CT} = 37.6\ \Omega\ cm^{-2}$ ($i_o = 6.8 \times 10^{-4}$ A cm^{-2}). Apparently, *o*-$LiMnO_2$ phase transfers to the spinel-like phase during the charging process and this electrochemically formed spinel-like phase is more reactive than that of the original *o*-$LiMnO_2$ phase. Two semicircles were observed in the charged state (4.2 V). Due to the reaction between the electrolyte and the surface of the

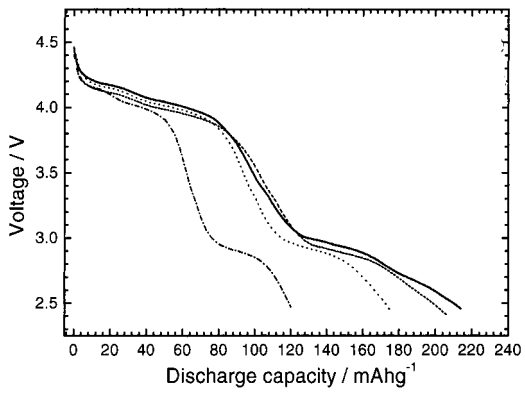

Fig. 7. Maximum discharge capacity of Li/*o*-$LiMnO_2$ cells at different discharge rates. Key: (–·–·–·) $C/4$ (15th cycle); (·····) $C/12$ (8th cycle); (- - - -) $C/50$ (2nd cycle); (——) $C/120$ (1st cycle).

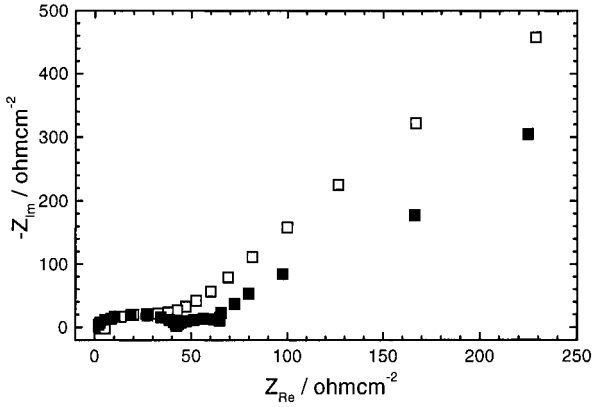

Fig. 8. a.c. impedance spectra of *o*-$LiMnO_2$ electrode at OCV state (3.25 V) and charged state (4.2 V). SOC: (□) 0% (3.25 V) and (■) 90% (4.2 V).

electrode, a surface layer formed on the electrode could be responsible for this second semicircle [19]. The formation of the surface layer consumes the electrolyte and the active materials. If it is not robust enough, it will be gradually damaged during the subsequent charge/discharge cycle. Therefore, the capacity of the electrode will decrease with cycling. This mechanism possibly contributes to the capacity loss of *o*-$LiMnO_2$ electrode on cycling.

4. Conclusions

The electrochemical properties of orthorhombic $LiMnO_2$ as the cathode in lithium cells were investigated. A maximum capacity in the range 180–190 mA h g^{-1} for *o*-$LiMnO_2$ electrode may be reached with fairly good cyclability. The kinetic characterisation of the electrode process by a.c. impedance spectroscopy showed the spinel-like phase transformed from *o*-$LiMnO_2$ more electrochemically active than that of the original *o*-$LiMnO_2$. *o*-$LiMnO_2$ is a promising cathodic material for rechargeable lithium batteries.

Acknowledgements

Financial support from Department of Employment, Education, Training and Youth Affairs, Australia, through the Targeted Institutional Links Program, is gratefully acknowledged.

References

1. J.M. Tarascon, W.R. McKinnon, F. Coowar, T.N. Bowmer, G. Amatucci and D. Guyomard, *J. Electrochem. Soc.* **141** (1994) 1421.
2. V. Manev, B. Banov, A. Momchilov and A. Nassalevska, *J. Power Sources* **57** (1995) 99.
3. W. Ebner, D. Fouchard and L. Xie, *Solid State Ionics* **69** (1994) 238.
4. R. Yazami, N. Lebrun, M. Bonneau and M. Molteni, *J. Power Sources* **54** (1995) 389.
5. A.R. Armstrong and P.G. Bruce, *Nature* **381** (1996) 499.
6. R.J. Gummow and M.M. Thackeray, *J. Electrochem. Soc.* **141** (1994) 1176.
7. I. Kötschau, M.N. Richard and J.R. Dahn, *J. Electrochem. Soc.* **142** (1995) 2906.
8. E. Levi, E. Zinigrad, H. Teller, M.D. Levi and D. Aurbach, *J. Electrochem. Soc.* **144** (1997) 4133.
9. I.J. Davidson, R.S. McMillan, J.J. Murray and J.E. Greedan, *J. Power Sources* **54** (1995) 232.
10. L. Croguennec, P. Deniard, R. Brec, P. Biensan and M. Broussely, *Solid State Ionics* **89** (1996) 127.
11. A. Lecerf, P. Biensan and S. Baudry, *French Patent 9 308 484* (1993) and *US Patent us 5 561 006* (1994).
12. L. Croguennec, P. Deniard and R. Brec, *J. Electrochem. Soc.* **144** (1997) 3323.
13. I.M. Kötschau and J.R. Dahn, *J. Electrochem. Soc.* **145** (1998) 2672.
14. L. Croguennec, P. Deniard, R. Brec and A. Lecerf, *J. Mater. Chem.* **7** (1997) 511.
15. T. Uchida, Y. Morikawa, H. Ikuta and M. Waikihara, *J. Electrochem. Soc.* **143** (1996) 2606.
16. Yuan Gao and J.R. Dahn, *J. Electrochem. Soc.* **143** (1996) 101.
17. M.M. Thackeray, *J. Electrochem. Soc.* **142** (1995) 2558.
18. B. Garcia, J. Farcy, and J.P. Pereira-Ramos, *J. Electrochem. Soc.* **144** (1997) 1179.
19. P. Arora, B.N. Popov and R.E. White, *J. Electrochem. Soc.* **145** (1998) 807.